Crystallinity Segregation upon Selective Self-Assembling of Gold Colloidal Single Nanocrystals

ARTICLE *in* NANO LETTERS · SEPTEMBER 2012

Impact Factor: 13.59 · DOI: 10.1021/nl3029009 · Source: PubMed

NANO LETTERS

Letter

pubs.acs.org/NanoLett

Crystallinity Segregation upon Selective Self-Assembling of Gold Colloidal Single Nanocrystals

Hervé Portalès,*[,†,‡] Nicolas Goubet,[†,‡] Sergey Sirotkin,[§] Eugène Duval,[§] Alain Mermet,[§] Pierre-Antoine Albouy,[∥] and Marie-Paule Pileni*[,†,‡]

[†]Université Pierre et Marie Curie Paris 6, UMR 7070, LM2N, BP 52, 4 place Jussieu, 75005 Paris, France

[‡]Centre National de la Recherche Scientifique, Unité Mixte de Recherche 7070, LM2N, 4 place Jussieu, 75005 Paris, France

[§]Université de Lyon, Université Lyon 1, LPCML, Unité Mixte de Recherche 5620, Bât. A. Kastler, 10 rue Ada Byron, 69622 Villeurbanne, France

[∥]Université Paris-Sud, LPS, Unité Mixte de Recherche 8502, 91405 Orsay, France

S *Supporting Information*

ABSTRACT: Spontaneous separation of single from polycrystalline 5 nm gold nanocrystals (NCs) is observed in colloidal solution. This segregation takes place upon self-assembling of single crystalline NCs at the air−solvent interface and in precipitated superlattices. Polycrystalline NCs are observed to remain in the suspension. Transmission electron microscopy analysis of the size distribution of NCs issued from the different populations indicates that the NC size does not change from each other, excluding therefore any size segregation in this process. Using both low-frequency Raman scattering and X-ray diffraction provides reliable characterization of nanocrystallinity for each population of NCs, thus confirming the crystallinity segregation. The single crystalline NCs are found by electron diffraction to self-assemble into close-packed superlattices with long-range translational and orientational ordering, while polycrystalline NCs behave like spheres with no preferential orientation. The face-to-face orientational ordering, which is only observed for single crystalline NCs, supports the relevance of the specific crystallinity-related morphologies of these NCs in their better ability to self-assemble. Exploiting this spontaneous segregation would open up a simple alternative to other demanding routes for controlling crystallinity of nanocrystals and optimizing their properties for potential applications.

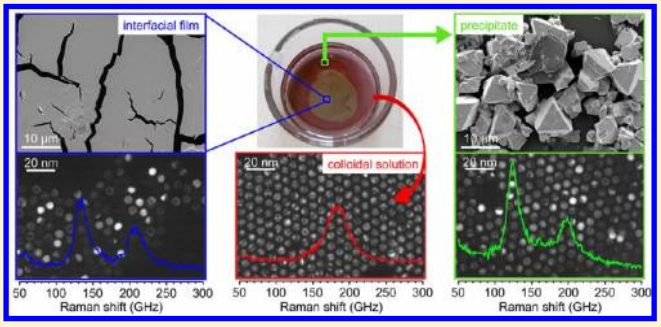

KEYWORDS: *Compact superlattice, self-assembly, facets, interface, anisotropy, orientational ordering*

Since the pioneer studies of nanocrystal (NC) superlattices,[1−3] these ordered assemblies of nanosized objects are experiencing rapidly increasing attention of chemists and physicists whose interest in this class of materials arises from both technological and fundamental standpoints. NC superlattices constitute ideal systems for studying novel chemical and physical properties originating from the collective interaction between NCs. In this regard, the relevance of using noble-metal NCs as building blocks lies in the dependence of their individual properties on their size, shape, composition, and on the surrounding medium. Such high sensitivity of noble-metal NC properties allows exploiting them for plasmonic, sensing and spectroscopic applications.[4,5] Optimization of the properties of close-packed NC assemblies requires nevertheless to properly control the superlattice structure on a nanometer-length-scale. Consequently, optimal use of these systems requires that the NC material's quality itself be controlled, encompassing not only uniformity in size, but also in other parameters like their shape and internal atomic lattice structure, which will be hereafter referred to as nanocrystallinity. Advances in the synthesis of colloidal metal NCs permit nowadays to exercise such fine control over their chemical composition, size and shape,[6−9] thus making it possible to self-assemble monodisperse quasi-spherical[10−13] as well as anisotropic[14−16] building blocks into superlattices.

Provided that NCs should exhibit closely matched morphological attributes and narrow size distribution, interesting phenomena are expected when assembling anisotropic NCs in well-ordered superlattices. As an example, due to shape-segregation during the crystallization process, polyhedral NCs have been observed to self-assemble in orientation-ordered superlattices.[17−19] Such a concept of inherent shape-directed crystallization was in particular examined in assemblies of DNA-functionalized nanoparticles wherein directional bonding interactions between the nanoparticles can be facilitated by their anisotropy.[15] More surprisingly, anisotropy effects have

Received: July 12, 2012
Revised: September 14, 2012
Published: September 18, 2012

dx.doi.org/10.1021/nl3029009 | *Nano Lett.* 2012, 12, 5292−5298

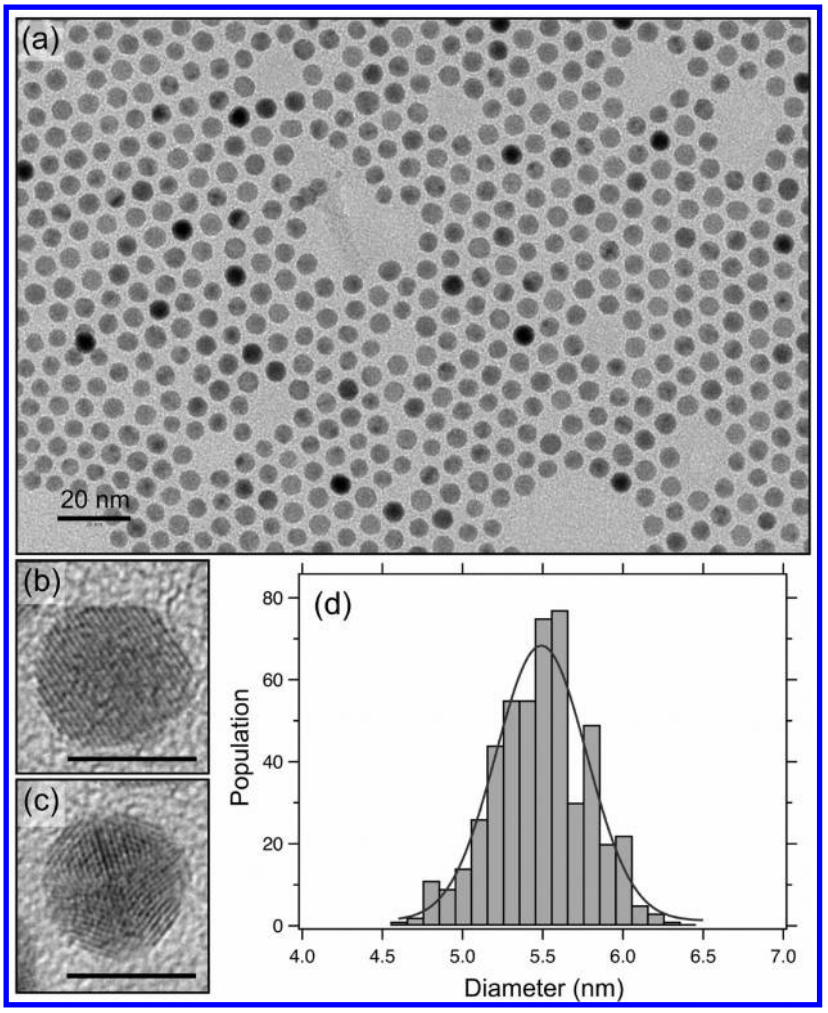

Figure 1. (a) Bright-field TEM image of a mixed population of single and polycrystalline Au NCs. HRTEM images showing one example of (b) monodomain and (c) polycrystalline NCs. The scale bars in the panels (b) and (c) represent 5 nm. (d) Size histogram determined by TEM analysis over a population of 500 Au NCs plotted along with a curve derived by fitting its profile with a Gaussian function.

been also observed in self-ordered assemblies of colloidal monodisperse metal NCs composed of building blocks with quasi-spherical morphology. For instance, the orientational ordering observed in superlattices of alkylthiolate passivated Ag NCs was ascribed to the NC's faceted morphology.[20] From another study, single and polycrystalline dodecanethiol-stabilized Au NCs prepared by different methods and with similar average size were observed to self-organize into different superlattice structures.[12] These results therefore suggested the ability of single and polycrystalline Au NCs to exhibit different packing behaviors depending upon their faceted morphology. As already known, Au NCs with different morphological attributes can be separated by depletion-induced size and shape selection through the formation of reversible flocculates in multicomponent colloidal solutions.[21] However, up to date, no segregation from the same batch of quasi-spherical NCs has been yet reported as resulting from the effect of nanocrystallinity on their self-assembling.

In this Letter, we report on spontaneous nanocrystallinity segregation observed in colloidal solution containing a mixed population of single and polycrystalline 5 nm NCs. This segregation proceeds upon selective self-assembling of single crystalline Au NCs into a thin film of NCs, growing at the air−toluene interface, or into precipitated three-dimensional close-packed superlattices, also called precipitated supracrystals. The single crystalline NCs assemble apart from their polycrystalline counterparts, which tend to remain in the suspension, as demonstrated through the characterization of their nanocrystallinity using low-frequency Raman scattering and X-ray diffraction. Transmission electron microscopy analysis of the diameter distribution of NCs issued from the different populations reveals that the NC size remains the same from each other, thus permitting to exclude the NC size as potential contributing factor in the segregation process. Further analysis by electron diffraction reveals the tendency of single crystalline NCs to self-assemble with orientational ordering and thereby confirming the relevance of NC faceting and shape in crystallinity segregation.

Colloidal Au NCs were synthesized as follows.[9] Briefly, two solutions were prepared in parallel. The first one was obtained by dissolving 0.25 mmol of chlorotriphenylphosphine gold(I) (Strem, 98%) in 25 mL of toluene (Riedel-deHaën, >99.5%) and then adding 500 mL of 1-dodecanethiol (Aldrich, ≥98%). To prepare the second solution, 5 mmol of tert-butylamine borane complex (Strem, >97%) were dissolved in 2 mL of toluene. Both solutions were stirred in a silicone bath heated at 100 °C to ensure the complete dissolution of all solid products. After having reached the bath temperature, these solutions were

dx.doi.org/10.1021/nl3029009 | Nano Lett. 2012, 12, 5292−5298

mixed together. At this stage, the color of the mixture was observed to progressively turn from brown to dark red due to the reduction of Au complex and to the subsequent NC growth inside the solution. After 5 min, the solution was removed from the bath and slowly cooled down to room temperature. At the end of the reduction process, Au NCs were washed with ethanol to eliminate byproduct and then redispersed in neat toluene.

Figure 1a shows the bright-field transmission electron microscopy (TEM) image of Au NCs issued from the as-synthesized colloidal solution after dropping it onto a carbon-coated copper grid (200 mesh). Bright-field and conical dark-field TEM analyses were performed using a JEOL 2010 (200 kV) microscope. For the conical dark-field TEM analysis, the motion of precession of the tilted electron beam was set to a frequency of 1.6 Hz. Both single and polycrystalline NCs are present in large amount, as deduced from the significant proportion of NCs exhibiting whether homogeneous or inhomogeneous contrast, respectively (see Figure S1 presented as Supporting Information). The coexistence of these two species is also evident when looking at the atomic lattice structure of NCs by high-resolution transmission electron microscopy (HRTEM). As typical examples, Figure 1b,c shows NCs with single domain and multiple twinned structures, respectively. Since both single and polycrystalline NCs are hereby demonstrated to coexist in the as-synthesized batch of NCs, one can therefore consider their nanocrystallinity as being uncontrolled. From the histogram plotted in Figure 1d characterizing the size distribution of the synthesized NCs, their average diameter is found to be $\langle D \rangle$ = 5.5 nm with size dispersion not exceeding 6%. Details on how the samples were prepared for their characterization by different techniques are given as Supporting Information.

After keeping the colloidal solution in a glass beaker under toluene atmosphere for 7 days, one observes the surface of the solution becoming slightly opaque with a gold metallic coloration. This slow change in coloration at the surface of the solution actually originates from the progressive growth of a thin NC film at the interface air−toluene, as it will be shown below using scanning electron microscopy (SEM). In parallel, at the bottom of the glass beaker a precipitate is formed by sedimentation of micrometer-sized close-packed arrays of Au NCs. A photograph clearly showing such a precipitate is given as Supporting Information in Figure S2. For simplicity, in the following the interfacial and precipitated NC superlattices will be referred to as interfacial and precipitated supracrystals. Figure 2a schematically represents the segregation inside the colloidal solution that gives rise to the different coexisting subsystems described above. The film of interfacial supracrystals is shown in Figure 2b. The photograph shown in Figure 2c illustrates the removal of the film from the air−toluene interface using a tungsten ring and its transfer onto a Si substrate (see also the movie presented as Supporting Information). After removing the interfacial and precipitated supracrystals from the beaker, the colloidal solution was evaporated and the NCs that remained in suspension were deposited on a silicon substrate. The deposition of the remaining NCs induced by the total evaporation of the solvent resulted in the formation of a film composed of self-assembled NCs, which will be called remaining supracrystals. Small-angle X-ray diffraction measurements performed on interfacial, precipitated and remaining supracrystals recently shown that

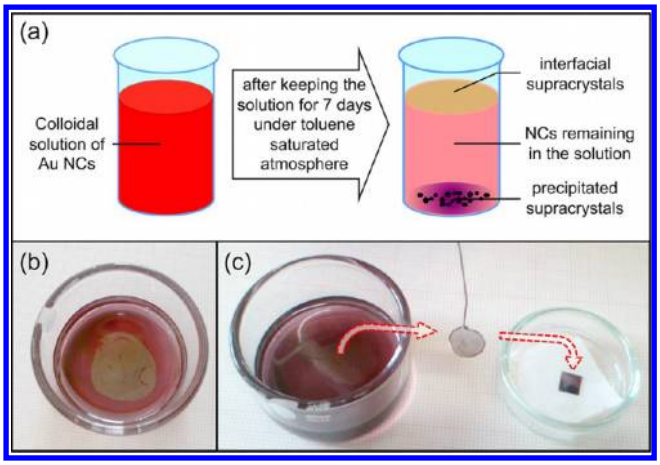

Figure 2. (a) Scheme illustrating the formation of the interfacial and precipitated supracrystals in the colloidal solution. Although the solution slightly discolors, its persistent coloring indicates the presence of NCs in the suspension. (b) Photograph of the NC film grown at the air−toluene interface. (c) Removal of interfacial supracrystals from the solution using a tungsten ring followed by their transfer/deposition onto a silicon substrate on the right side (photograph extracted from the movie presented as Supporting Information).

all of them are composed of NCs self-ordered in face-centered cubic (fcc) structure.[13]

The SEM images of these supracrystals reveal distinct architectures from one segregated subsystem to the other (see Figure S3 given as Supporting Information). In particular, most precipitated supracrystals exhibit polyhedral geometries. At variance, interfacial supracrystals are composed of NCs self-assembled into thin planar arrangements to form a film whose apparent homogeneous thickness ranges typically between 200 and 300 nm depending on the concentration of the Au colloidal solution. In comparison to the interfacial film, more internal defects are observed in the film composed of remaining supracrystals.

Further observation at the nanometer scale performed by conical dark-field TEM of NCs originating from each segregated population provides very interesting and unexpected information on nanocrystallinity. Most NCs issued from the interfacial film and the precipitated supracrystals (see Supporting Information Figure S3) are observed to exhibit either single crystalline or poorly twinned structures. Conversely, a large proportion of the remaining NCs is composed of multiply twinned particles (MTPs) and only few single crystalline NCs are visible. On the basis of the above-mentioned TEM images, it can be reasonably deduced that Au NCs segregate according to their nanocrystallinity. As a matter of fact, there appears to be a correlation between good crystallinity and self-assembling of single NCs into either interfacial or precipitated supracrystals, as opposed to poor nanocrystallinity and remaining of polycrystalline NCs in the solution. Nevertheless, only local and therefore limited information is provided by TEM observation. To ascertain the crystallinity segregation based on a broader statistical ensemble, additional data are presented hereafter using another method allowing for the fine characterization of nanocrystallinity from a large population of NCs.

Low-frequency Raman scattering (LFRS) by Au NCs was recently demonstrated to significantly depend on nanocrystallinity.[22] Accordingly, LFRS measurements should be able to ensure that most interfacial and precipitated NCs are

dx.doi.org/10.1021/nl3029009 | Nano Lett. 2012, 12, 5292−5298

single crystalline, as anticipated from TEM observations. Conversely, one expects the vibrational response of NCs from the remaining supracrystals to be similar to that usually observed for multiple twinned or polycrystalline particles. The LFRS measurements reported here were performed at room temperature using as excitation source either the green line at 532 nm or the yellow line at 561 nm of diode pumped solid-state lasers. Each spectrum was recorded by detecting the scattered light in a classical backscattering geometry using a six-pass tandem Fabry-Pérot interferometer[23] coupled with a Si avalanche photodiode.

The Stokes/anti-Stokes LFRS spectra of interfacial, remaining, and precipitated Au NCs recorded for an excitation at 532 nm are plotted in Figure 3. The unique broad band, which is

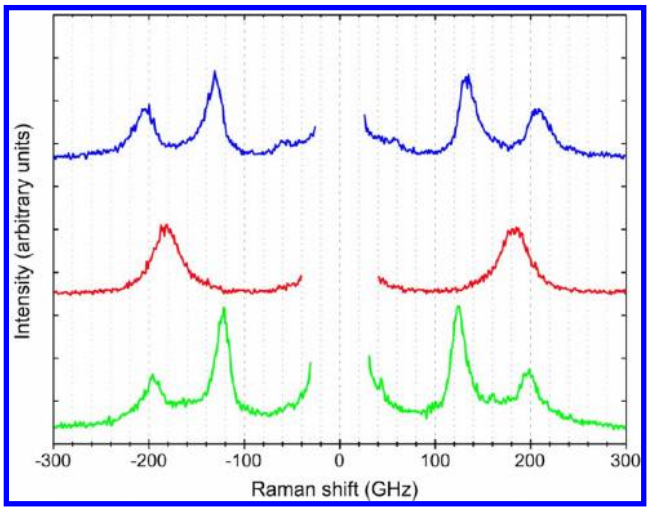

Figure 3. Stokes and anti-Stokes LFRS spectra of interfacial (top blue curve), remaining (medium red curve), and precipitated (bottom green curve) Au NCs recorded using an excitation wavelength of 532 nm. For clarity, the spectra have been independently scaled and vertically shifted.

centered at around 180 GHz in the spectrum of Au NCs remaining in the solution (middle spectrum), corresponds to resonant Raman scattering by acoustic quadrupolar vibrations of these NCs as a result of their efficient coupling at this excitation wavelength with localized surface plasmons.[24,25] The quadrupolar mode is simply identified here by its angular momentum number $l = 2$, as only the fundamental mode is observed in the presented Raman spectra. At variance, for interfacial and precipitated supracrystals (top and bottom curves), the LFRS spectra exhibit two bands peaked at frequency shifts of around 130 and 200 GHz. These two bands are attributed to the Raman scattering by the same $l = 2$ quadrupolar mode as mentioned before except that this 5-fold degenerate mode is split into two components in the case where the NCs are single crystalline, that is, when one has to consider the anisotropy of the elastic tensor in the fcc structure. These two components are the 2-fold degenerate E_g mode and the 3-fold degenerate T_{2g} mode, in increasing order of vibrational frequencies.

The band assignment given above is further confirmed by comparing quantitatively in Table 1 the measured vibrational frequencies to those calculated using the resonant ultrasound (RUS) approach[26,27] (see also Figure S4 and Table S1 given as Supporting Information). From a computational point of view, using this method allows one to take into account the

Table 1. Comparison of Frequencies Calculated for the E_g, T_{2g}, and $l = 2$ Quadrupolar Vibrational Modes of Au Spheres with Different Diameters, D, Using the RUS Approach to Those Measured Using an Excitation at 532 nm for NCs Issued from Interfacial, Remaining, and Precipitated Supracrystals

	calculated frequencies/GHz			measured frequencies/GHz		
modes	D = 5.5 nm	D = 5.7 nm	D = 5.9 nm	interfacial NCs	remaining NCs	precipitated NCs
E_g	136	131	126	132		124
$l = 2$	192	186	179		183	
T_{2g}	219	211	204	206		196

anisotropy of the stiffness tensor of gold to calculate the vibrational mode frequencies of Au single NCs. Besides, the twinning of polycrystalline NCs is accounted for by using an isotropic approximation of gold that consists in averaging the sound velocities over the three spatial dimensions. Thus, the averaged longitudinal and transverse sound velocities of this fictive isotropic material were estimated to be 3330 and 1250 m/s, respectively. Actually, it should be noted that polycrystalline NCs are not expected to individually vibrate like elastically isotropic nanoparticles but due to different number and position of twins from one NC to the other their ensemble can be satisfactorily described by using such isotropic approximation.[22]

As deduced from the comparison given in Table 1, the frequencies calculated for Au nanospheres with the same diameter as the one determined by TEM analysis (i.e., $\langle D \rangle$ = 5.5 nm) are found to overestimate by 4−6% the vibrational frequencies of interfacial NCs and by 10−12% those measured in precipitated NCs. A better fit of the measured frequencies is obtained when modeling Au NCs by nanospheres with diameter of 5.7 or 5.9 nm. The fairly good agreement between the measured frequencies and those calculated for NCs with diameter slightly larger than the average experimental one could be tentatively interpreted by a NC size segregation that would take place in the interfacial film and the precipitate. To test this assumption, the size histograms characterizing the different populations of NCs were determined by TEM analysis. The comparison of the histograms presented in Figure 4 reveals that no sensitive variation in NC size was actually found between the three segregated populations. Indeed, the variation by only 0.1 nm observed between the average diameter of the remaining NCs and the other ones is much smaller than the size dispersion derived for each population from the fit of the histograms by a Gaussian function. From this comparison, one can accurately exclude any size discrepancy between single and polycrystalline NCs as being responsible for their segregation.

The mismatch between measured and calculated frequencies could reveal the influence of the local environment of NCs on their vibrations. Indeed, the close packing of NCs in supracrystals and their mechanical contact via the coating molecules probably affect their vibrational motions that can no more be rigorously simulated using the model of a free elastic sphere. According to previous studies,[28] an effect of vibrational coherence between nanocrystals self-organized in supracrystals could also explain the observed small red shift of the NC vibration frequencies. Anyway, the model used for calculating these frequencies would ideally require some refinement to

dx.doi.org/10.1021/nl3029009 | Nano Lett. 2012, 12, 5292−5298

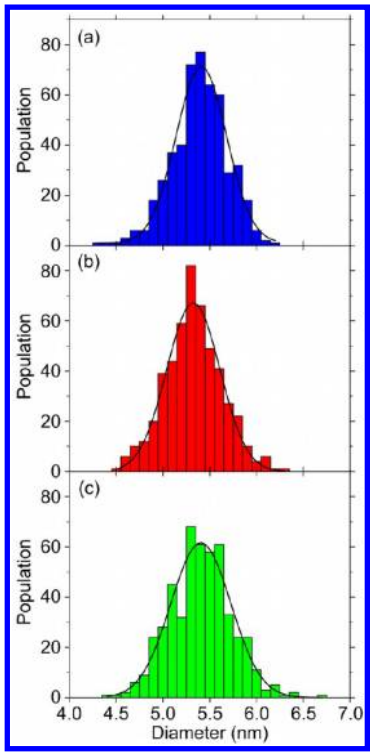

Figure 4. Size histograms characterizing the populations of (a) interfacial, (b) remaining and (c) precipitated NCs. Each histogram is determined by TEM analysis over an ensemble of 500 NCs. The average diameter was derived by a fit with a Gaussian profile (black curve) and was found to be (a) 5.4 ± 0.6 nm, (b) 5.3 ± 0.6 nm, and (c) 5.4 ± 0.6 nm.

better account for the mutual influence of neighboring NCs in such close-packed arrangements. However, looking at the small difference of only a few percent between the calculated and measured frequencies, one reasonably concludes that the individual vibrations of the studied NCs remain weakly affected by their compact self-assembling in supracrystals.

From Table 1, it should also be noticed that the measured frequencies are systematically smaller in precipitated compared to interfacial NCs for a given mode. On the basis of recent nanoindentation measurements, the Young's modulus was estimated to be of the order of few GPa and more than five times larger in precipitated as compared to interfacial supracrystals.[13] The higher stiffness in the precipitated supracrystals results from different growth mechanism and presumably stronger mechanical coupling between NCs. The slight difference in the vibrational frequencies of precipitated and interfacial NCs could therefore be due to different strength of the mechanical coupling between NCs in these two systems.

To definitely attest to the crystallinity segregation between single and polycrystalline NCs, X-ray diffraction (XRD) measurements were performed on a homemade setup. Briefly speaking, it consists in vacuum chamber mounted on a rotating anode generator (copper anode: λ = 0.1542 nm). Monochromatization of the X-ray beam is ensured by a graded multilayer optics that delivers a parallel beam. X-ray spectra are recorded onto photostimulable imaging plates. Working under vacuum with suitable collimator and beam-stop considerably reduces parasitic scattering so that very small samples can be probed. Because of the presence of structural defects, the size of the domains inside polycrystalline NCs is likely to significantly differ from the whole NC size, in contrast to the case of single crystalline NCs. Powder X-ray diffraction is sensitive to the domain size, which therefore makes this technique suitable for characterizing nanocrystallinity. In particular, XRD experiments allow to estimate the domain size in NCs.[29] Following ref 30 and assuming spherical nanoparticles, we can estimate the volume average diameter $\langle D\rangle_{XRD}$ from the volume average column length $\langle L\rangle_{vol}$ using the simple equation $\langle D\rangle_{XRD} = (4/3)\langle L\rangle_{vol}$. An estimation of $\langle L\rangle_{vol}$ is given by the Scherrer formula

$$\langle L\rangle_{vol} = \frac{0.9\lambda}{w\cos\theta} \quad (1)$$

where θ is the Bragg angle of the considered diffraction peak, w its width on a 2θ scale and λ is the wavelength of the radiation. The powder X-ray diffractograms of Au NCs issued either from interfacial, remaining or precipitated supracrystals are shown in Figure 5. For each case, the width of the most intense {111}

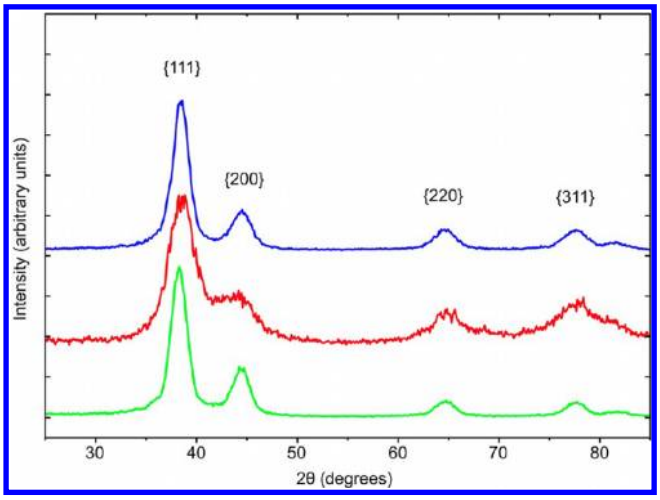

Figure 5. Powder X-ray diffractograms of Au NCs issued from interfacial (top blue curve), remaining (medium red curve), and precipitated (bottom green curve) supracrystals. The diffractograms have been independently scaled and vertically shifted.

peak was estimated by a fit with a Lorentzian profile. The diameters of interfacial and precipitated NCs obtained by this procedure were found to be 4.9 and 5.2 nm, respectively, which are close to those estimated by TEM analysis, thus confirming these NCs as being mostly monodomain. Fitting the powder XRD pattern of remaining NCs provided a value of only 3.2 nm in contrast to the corresponding TEM diameter of 5.3 nm (Figure 4). The mismatch between the TEM and XRD diameters observed in this last case is due to twinning and structural defects in remaining NCs and the resulting decrease in coherence length. Note that the presence of grains with smaller size in remaining NCs induces noisier signal in their diffractogram (Figure 5) compared to those of interfacial and precipitated NCs although all diffractograms were recorded using the same acquisition time.

As an attempt to find out the origin of the selective self-assembling of single NCs at the interface or in the precipitate, one proposes now to argue in favor of the crystallinity-related shapes of NCs as responsible for such crystallinity segregation. This assumption makes sense since no clear discrepancy in size was observed between single and polycrystalline NCs. The unexpected ability of these latter to selectively self-assemble

dx.doi.org/10.1021/nl3029009 | Nano Lett. 2012, 12, 5292−5298

apart from the polycrystalline NCs could therefore not be simply due to size segregation.

It should be noted here that MTPs, whose presence in our sample was demonstrated by TEM (see Supporting Information Figure S1), are well-known to exhibit either decahedral or icosahedral shapes.[31] The decahedral and icosahedral MTPs are fully enclosed by uniformly sized triangular facets corresponding to {111} crystallographic surfaces. On the other side, the possible shapes of single NCs were described by the Wulff construction,[32] which is a reliable tool for predicting the most energetically stable clusters in single-component systems beyond a few hundred atoms. Among the variety of existing shapes, two typical examples of commonly observed shapes for metal single NCs with fcc structure are the cuboctahedron and the truncated octahedron, where both {111} and {100} facets are present,[33] which is in contrast with decahedral and icosahedral MTPs. Depending on their crystallographic surface, the facets of a single NC not only differ in shape and size but also in surface energy and atom density. As a consequence, the electronic and bonding properties of the facets should naturally also depend on their crystallographic surface. Such variation in the facet properties from one crystallographic surface to the others is likely to dictate the respective ability of MTPs and single NCs in interacting with their environment via the coating molecules. Additionally, the presence of facets in typical morphologies of single NCs with relatively larger area than the facets of MTPs could also play a key role in the crystallinity segregation by strengthening the interactions between single NCs, thus favoring their self-assembling.

To support the previous argumentation, low- and high-angle electron diffraction data are now presented. This characterization was performed using a transmission electron microscope JEOL 1011 (100 kV). For high-angle diffraction, the camera length was either 10 or 20 cm while it was increased to 250 cm for low-angle diffraction. In the inset of Figure 6a, one shows the low-angle electron diffraction pattern recorded from a thin film of single Au NCs obtained after drying a droplet of colloidal solution on a TEM grid. The hexagonal symmetry of the diffraction pattern confirms the compact structure of the NC superlattice. The high-angle diffraction pattern presented in Figure 6a exhibits several rings corresponding to electron diffraction by specific planes of atomic lattices with fcc structure. In this pattern, small arcs are distinctly observed for most diffraction rings. Similar arcs in the high-angle diffraction pattern were previously observed in superlattices of self-assembled nonspherical building blocks,[16] and especially consisting of Ag[20] and Au[11,12] NCs. Such a feature provides evidence for an average coherent alignment of the atomic lattice planes of NCs to one another within the superlattice. This orientational ordering of the atomic lattices of Au NCs is indicative of their faceted morphology and is presumably favored by large facets in single NCs. These latter facets are indeed expected to exhibit large enough area to induce their face-to-face orientation between neighboring NCs despite the presence of dodecanethiol molecules tethered to their surface. In contrast, when looking at the high-angle diffraction pattern obtained from polycrystalline NCs (Figure 6b), diffraction rings exhibit no similar arcs as those previously mentioned although these NCs are also close-packed in compact superlattice, as shown by the inset in Figure 6b. This result means that polycrystalline NCs self-assemble into arrays with long-range translational but no orientational ordering and confirms previous observations from Au NC superlattices whose

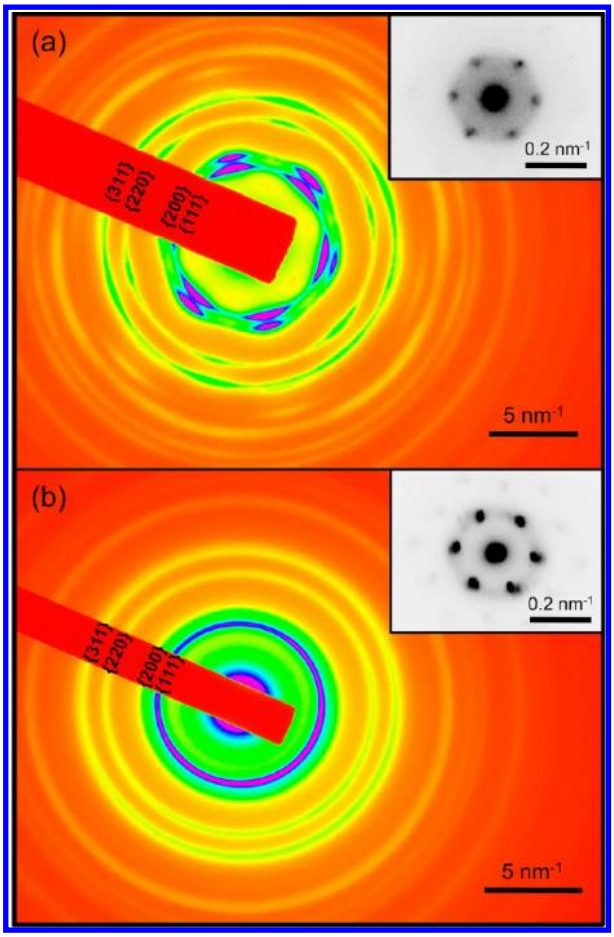

Figure 6. High-angle electron diffraction patterns recorded from a thin film of close-packed (a) single crystalline and (b) polycrystalline Au NCs. In (a) and (b), the patterns are colored to help in viewing the arcs and diffractions by {111}, {200}, {220}, and {311} planes are indexed. Insets in (a) and (b) show the low-angle electron diffraction patterns recorded from self-assembled single crystalline and polycrystalline Au NCs, respectively.

structures were found to depend upon the crystallinity of the nanocrystals via the method used for their preparation.[12] Actually, in addition to the crystallinity of NCs and their inherent shape anisotropy, the van der Waals interactions between the surfactant chains and their possible directional distribution should also play an important role in the orientational ordering of NCs, as suggested by previous studies on Ag NC superlattices.[10,20] The crystallinity segregation of colloidal faceted NCs can be therefore ascribed to a shape-directed crystallization process mediated by the interactions of surfactant molecules tethered on the facets of neighboring NCs.

In summary, a colloidal solution containing a mixed population of Au single and polycrystalline nanocrystals of around 5 nm in diameter is synthesized using an organometallic route. Formation of a thin supracrystal film at the surface of this colloidal solution and sedimentation of close-packed nanocrystal superlattices, called supracrystals, are observed after keeping the solution under toluene-saturated atmosphere for seven days. By use of low-frequency Raman scattering and X-ray diffraction both the interfacial and precipitated supracrystals are demonstrated to be mainly composed of single NCs while those remained in the suspension are mostly polycrystalline. This finding points to a spontaneous crystallinity segregation in

dx.doi.org/10.1021/nl3029009 | *Nano Lett.* 2012, 12, 5292−5298

the colloidal solution upon selective self-assembling of single NCs. Determination of the diameter distribution by transmission electron microscopy for the different segregated populations allows excluding any size segregation in this process. Different packing behaviors between single and polycrystalline NCs are revealed by electron diffraction. After being deposited onto a substrate, single NCs are found to self-assemble into close-packed superlattices with long-range translational and orientational ordering, while polycrystalline NCs behave like spheres with no preferential orientation in the NC array. This difference in packing behavior clearly indicates the major role that crystallinity related faceting and shape anisotropy of nanocrystals play in the structure and subsequent properties of their superlattices. The crystallinity segregation reported in this work definitely reveals the direct influence of the morphology of nanocrystals on their ability to interact and self-assemble. The separation of single from polycrystalline NCs by such crystallinity segregation interestingly appears like an efficient alternative to the development of complex synthetic route for controlling nanocrystallinity.

■ ASSOCIATED CONTENT

Supporting Information

Details on the preparation of the samples for their characterization by XRD, electron diffraction, LFRS and SEM are available, as well as further information and images related to the structural analysis of nanocrystals by conical dark-field TEM. A photograph showing the formation of both the interfacial film and the precipitate in the colloidal solution and additional data of LFRS measurements are also available. This material is available free of charge via the Internet at http://pubs.acs.org.

■ AUTHOR INFORMATION

Corresponding Author

*E-mail: (H.P.) herve.portales@upmc.fr; (M.P.P.) marie-paule.pileni@upmc.fr.

Notes

The authors declare no competing financial interest.

■ ACKNOWLEDGMENTS

N.G. and H.P. thank S. Casale (Université Pierre et Marie Curie) for giving technical assistance in the characterization of the nanocrystals by conical dark-field TEM as well as HRTEM. The M.P.P. contribution to this research has received funding from an Advanced Grant of the European Research Council under Grant Agreement N° 267129.

■ REFERENCES

(1) Motte, L.; Billoudet, F.; Pileni, M. P. *J. Phys. Chem.* **1995**, *99* (44), 16425−16429.
(2) Murray, C. B.; Kagan, C. R.; Bawendi, M. G. *Science* **1995**, *270* (5240), 1335−1338.
(3) Brust, M.; Schiffrin, D. J.; Bethell, D.; Kiely, C. J. *Adv. Mater.* **1995**, *7* (9), 795−797.
(4) Willets, K. A.; Van Duyne, R. P. *Annu. Rev. Phys. Chem.* **2007**, *58*, 267−297.
(5) Cobley, C.; Skrabalak, S.; Campbell, D.; Xia, Y. *Plasmonics* **2009**, *4* (2), 171−179.
(6) Niu, W.; Zheng, S.; Wang, D.; Liu, X.; Li, H.; Han, S.; Chen, J.; Tang, Z.; Xu, G. *J. Am. Chem. Soc.* **2008**, *131* (2), 697−703.
(7) Zhang, Q.; Xie, J.; Yang, J.; Lee, J. Y. *ACS Nano* **2008**, *3* (1), 139−148.
(8) Seo, D.; Yoo, C. I.; Chung, I. S.; Park, S. M.; Ryu, S.; Song, H. *J. Phys. Chem. C* **2008**, *112* (7), 2469−2475.
(9) Goubet, N.; Richardi, J.; Albouy, P.-A.; Pileni, M.-P. *Adv. Funct. Mater.* **2011**, *21* (14), 2693−2704.
(10) Korgel, B. A.; Fullam, S.; Connolly, S.; Fitzmaurice, D. *J. Phys. Chem. B* **1998**, *102* (43), 8379−8388.
(11) Brown, L. O.; Hutchison, J. E. *J. Phys. Chem. B* **2001**, *105* (37), 8911−8916.
(12) Stoeva, S. I.; Prasad, B. L. V.; Uma, S.; Stoimenov, P. K.; Zaikovski, V.; Sorensen, C. M.; Klabunde, K. J. *J. Phys. Chem. B* **2003**, *107* (30), 7441−7448.
(13) Goubet, N.; Portalès, H.; Yan, C.; Arfaoui, I.; Albouy, P.-A.; Mermet, A.; Pileni, M.-P. *J. Am. Chem. Soc.* **2012**, *134* (8), 3714−3719.
(14) Glotzer, S. C.; Solomon, M. J. *Nat. Mater.* **2007**, *6* (7), 557−562.
(15) Jones, M. R.; Macfarlane, R. J.; Lee, B.; Zhang, J.; Young, K. L.; Senesi, A. J.; Mirkin, C. A. *Nat. Mater.* **2010**, *9* (11), 913−917.
(16) Quan, Z.; Fang, J. *Nano Today* **2010**, *5* (5), 390−411.
(17) Song, Q.; Ding, Y.; Wang, Z. L.; Zhang, Z. J. *J. Phys. Chem. B* **2006**, *110* (50), 25547−25550.
(18) Tao, A. R.; Ceperley, D. P.; Sinsermsuksakul, P.; Neureuther, A. R.; Yang, P. *Nano Lett.* **2008**, *8* (11), 4033−4038.
(19) Henzie, J.; Grünwald, M.; Widmer-Cooper, A.; Geissler, P. L.; Yang, P. *Nat. Mater.* **2012**, *11* (2), 131−137.
(20) Harfenist, S. A.; Wang, Z. L.; Alvarez, M. M.; Vezmar, I.; Whetten, R. L. *J. Phys. Chem.* **1996**, *100* (33), 13904−13910.
(21) Park, K.; Koerner, H.; Vaia, R. A. *Nano Lett.* **2010**, *10* (4), 1433−1439.
(22) Portales, H.; Goubet, N.; Saviot, L.; Adichtchev, S.; Murray, D. B.; Mermet, A.; Duval, E.; Pileni, M. P. *Proc. Natl. Acad. Sci. U.S.A.* **2008**, *105* (39), 14784−14789.
(23) Lindsay, S. M.; Anderson, M. W.; Sandercock, J. R. *Rev. Sci. Instrum.* **1981**, *52* (10), 1478−1486.
(24) Palpant, B.; Portales, H.; Saviot, L.; Lerme, J.; Prevel, B.; Pellarin, M.; Duval, E.; Perez, A.; Broyer, M. *Phys. Rev. B* **1999**, *60* (24), 17107−17111.
(25) Bachelier, G.; Mlayah, A. *Phys. Rev. B* **2004**, *69* (20), 205408.
(26) Visscher, W. M.; Migliori, A.; Bell, T. M.; Reinert, R. A. *J. Acoust. Soc. Am.* **1991**, *90* (4), 2154−2162.
(27) Saviot, L.; Murray, D. B. *Phys. Rev. B* **2009**, *79* (21), 214101.
(28) Courty, A.; Mermet, A.; Albouy, P. A.; Duval, E.; Pileni, M. P. *Nat. Mater.* **2005**, *4* (5), 395−398.
(29) Borchert, H.; Shevehenko, E. V.; Robert, A.; Mekis, I.; Kornowski, A.; Grubel, G.; Weller, H. *Langmuir* **2005**, *21* (5), 1931−1936.
(30) Natter, H.; Schmelzer, M.; Loffler, M. S.; Krill, C. E.; Fitch, A.; Hempelmann, R. *J. Phys. Chem. B* **2000**, *104* (11), 2467−2476.
(31) Ino, S.; Ogawa, S. *J. Phys. Soc. Jpn.* **1967**, *22*, 1365−1374.
(32) Wulff, G. *Krystallogr. Mineral.* **1901**, *34* (5/6), 449−530.
(33) Wang, Z. L. *J. Phys. Chem. B* **2000**, *104* (6), 1153−1175.